Transport and accumulation of organic matter in forward osmosis-reverse osmosis hybrid system: Mechanism and implications

Transport and Accumulation of Organic Matters in Forward Osmosis-Reverse Osmosis Hybrid System

Separation and Purification Technology

Revised: 24 April, 2016

Ming Xie [1*] and Stephen R. Gray [1]

[1] Institute for Sustainability and Innovation, College of Engineering and Science, Victoria University, PO Box 14428, Melbourne, Victoria 8001, Australia

*Corresponding author E-mail: ming.xie@vu.edu.au

ABSTRACT

The productivity and sustainability of forward osmosis (FO) – reverse osmosis (RO) system could be hindered by contaminant accumulation in the draw solution. A significant, progressive contaminant accumulation was observed when digested sludge was processed by the FO-RO system. The FO-RO system achieved stable water production and high rejections of dissolved organic matter; however, contaminant accumulation was evident by a progressive increase of contaminants in the draw solution. Mechanism for contaminant accumulation was elucidated by examining the passage and accumulation of dissolved organic matter using fluorescence excitation emission matrix (EEM) spectroscopy and size exclusion (SEC) chromatography. Contaminant that accumulated in the draw solution exhibited a distinct signature in the fluorescence EEM spectra at peak T_1, suggesting protein-like substance. The molecular weight of the protein-like substance was resolved by SEC chromatography, identifying a molecular weight of 200 g/mol. The molecular weight of the protein-like substance was between the estimated molecular weight cut-offs of RO and FO membranes. As a result, such low molecular weight protein-like substance diffused through the FO membrane, and was largely rejected by the RO membrane by the virtue of steric hindrance mechanism, thereby accumulating in the draw solution of the closed-loop FO-RO system.

Keywords: forward osmosis; reverse osmosis; contaminant accumulation; dissolve organic matter; steric hindrance

1. Introduction

Forward osmosis (FO), an osmosis-driven membrane process, could potentially advance wastewater treatment and reuse [1]. FO utilizes the osmotic pressure of a highly concentrated draw solution as the driving force to transfer water from the feed solution to the draw solution through a dense polymeric membrane. FO has demonstrated a much lower fouling propensity and higher fouling reversibility than RO, which was attributed to the lack of applied hydraulic pressure [2-5]. Consequently, FO is widely used to treat low quality feedwaters, including landfill leachate [6], anaerobic digester concentrate [7], activated sludge solution [8, 9], and municipal wastewater [10-12].

Re-concentrating diluted draw solution and producing purified water demand FO process to be coupled with a downstream process, such as nanofiltration (NF) [13], reverse osmosis (RO) [14-16], or membrane distillation (MD) [11, 12, 17, 18]. Generally, these hybrid systems purified either wastewater effluent or seawater by double membrane barriers, achieving high rejections of most contaminants. For instance, drinking water quality can be obtained by the FO-RO hybrid system when Hancock et al. [19] examined long-term performance of an FO-RO hybrid system processing 900,000 L of effluent from a membrane bioreactor.

The closed-loop FO-based process is challenged by contaminant accumulation in the draw solution. Indeed, there was a notable build-up of organic matter and micropollutants in the draw solution in an FO-MD system [11, 12]. This accumulation was mainly driven by the near complete rejection of non-volatile solutes by the MD membrane in the FO-MD hybrid system, thereby leading to an undesirable contaminant accumulation in the draw solution. A similar concept was also modelled in an FO-RO system, where the RO membrane has higher rejection than the FO membrane [20]. For example, D'Haese et al. [21] modelled micropollutant accumulation in an FO-RO hybrid system, and predicted that an elevated micropollutant concentration in the draw solution deteriorated the product water quality. However, the underlying mechanisms governing the contaminant accumulation phenomenon remain largely unknown.

The ability of FO-RO system to process digested sludge and recover valuable nutrients could provide a unique perspective to examine contaminant accumulation in the FO-RO system [11]. The complex constituents in digested sludge comprises high concentration

of nutrient ions (ammonium and phosphate), and a wide spectrum of dissolved organic matter whose concentrations were several orders of magnitude higher than wastewater effluent or seawater [22, 23]. This magnification allows us to precisely capture the passage through, and accumulation of these contaminants in the FO-RO system. For example, Valladares Linares et al. [23] employed liquid chromatography with organic carbon detector to examined the transport of dissolved organic matter through the FO membrane, and identified an increase in the low molecular weight organic substances in the draw solution at the conclusion of the experiment. In another study, Hancock et al. [19] used fluorescence excitation and emission matrix spectroscopy to monitor the draw solution quality where an increase in fluorescence signature of protein-like substances was observed. However, there lacked an in-depth examination of the transport of dissolved organic matter, and a comprehensive understanding of the underlying mechanism in the contaminant accumulation phenomenon in FO-RO system. Such knowledge can be instrumental to FO-based closed-loop system, as well as emerging osmotic membrane bioreactor where the contaminant and salinity build-up were a key issue in a sustainable operation.

The aim of this study is to investigate the mechanism of contaminant accumulation in the closed-loop FO-RO system processing low quality digested sludge feed. The passage and subsequent accumulation of nutrients and dissolved organic matter in the FO-RO membrane were examined and quantified. Species and the corresponding molecular weight of dissolved organic matter in the draw solution and permeate were characterised by fluorescence excitation and emission spectroscopy and size exclusion chromatography. Membrane pore radii and molecular weight cutoffs of FO and RO membrane were estimated and correlated to the characteristics of dissolved organic matter to delineate contaminant accumulation in the draw solution.

2. Materials and methods

2.1. Digested sludge feed

Anaerobically digested sludge was collected from an anaerobic digester of the Eastern Treatment Plant in Melbourne (Victoria, Australia). The sludge centrate was obtained by screening the sludge through a 0.5 mm sieve, then centrifuging at 4,500 rpm for 25 min (Avanti J-26S XPI, Beckman Coulter, Fullerton, CA). The centrate was kept at 4ºC and used within two weeks to ensure the consistent solution chemistry.

2.2. Forward and reverse osmosis membranes

A flat-sheet, polyamide thin-film composite membrane from Hydration Technology Innovations (Albany, OR) was used for the FO process. The FO membrane is made of a thin selective polyamide active layer on top of a porous polysulfone support layer [24, 25]. An RO membrane (SW30) was supplied by Dow FilmTec (Minneapolis, MN), which was made of a thin aromatic polyamide active layer and a thick, porous support layer. Key membrane transport parameters, membrane pore radii and molecular weight cutoffs were determined to elucidate the contaminant accumulation phenomenon in the FO-RO system.

2.2.1. Key mass transfer parameters

Key membrane transport parameters were characterised following the protocol previously described by Cath et al. [25], including the pure water permeability coefficient of the active layer, *A*, and the salt (NaCl) permeability coefficient of the active layer, *B*. Briefly, the membrane *A* and *B* values were determined using a laboratory RO cross-flow filtration system (section 2.3). The membrane *A* value was measured at a pressure of 10 bar using deionised water. NaCl was then added to the feed solution to determine the *B* value. The RO system was stabilised for two hours before recording permeate water flux with 2000 mg/L NaCl solution, J_w^{NaCl}, and taking feed and permeate samples to determine the observed NaCl rejection, R_o. The membrane *A* value was calculated by dividing the pure water permeate flux (J_w^{RO}) by the applied hydraulic pressure, ΔP:

$$A = J_w^{RO} / \Delta P \qquad (1)$$

The observed salt (NaCl) rejection, R_o, was calculated from the difference between the bulk feed (c_b) and permeate (c_p) salt concentrations, $R_o = 1 - c_p/c_b$, and then the membrane B value was determined from:

$$B = J_w^{NaCl}\left(\frac{1-R_o}{R_o}\right)\exp\left(-\frac{J_w^{NaCl}}{k_f}\right) \qquad (2)$$

where k_f is the mass transfer coefficient for the cross-flow of RO membrane cell.

The mass transfer coefficient (k_f) was experimentally determined using the Sutzkover et al. method [26]. Using the permeate and feed salt concentrations (and thus, the corresponding osmotic pressures based on van't Hoff equation, π_p and π_b, respectively), the applied pressure (ΔP), the pure water flux (J_w^{RO}), and the permeate flux with the 2,000 mg/L NaCl solution (J_w^{NaCl}) enabled the evaluation of the salt concentration at the membrane surface. This membrane surface concentration was used with thin-film theory for concentration polarization to determine k_f:

$$k_f = \frac{J_w^{NaCl}}{\ln\left[\frac{\Delta P}{\pi_b - \pi_p}\left(1-\frac{J_w^{NaCl}}{J_w^{RO}}\right)\right]} \qquad (3)$$

2.2.2. Estimation of average membrane pore radius

A set of inert, neutral organic tracer – erythritol, xylose, and glucose (Sigma-Aldrich, Saint Louis, MO) – were used to estimate the membrane average pore radius. These organic tracers are neutrally charged, and do not adsorb to the membrane. As a result, they do not have a specific attractive or repulsive interaction with the membrane. The solutes were individually dissolved in Milli-Q water to obtain a concentration of 50 mg/L (as total organic carbon (TOC)). Prior to the RO filtration experiments with these reference organic solutes, the membrane was pre-compacted at 18 bar for one hour and subsequent experiments were conducted at 8, 10, 12, 14, and 16 bar with a cross-flow velocity of 9 cm/s. At each pressure value, the RO filtration system was operated for one hour before taking permeate and feed samples for analysis. This pressure range ensured that the organic tracer rejection can be clearly distinguished at a reasonable permeate flux range.

The membrane average pore radius was determined based on the pore hindrance transport model previously described by Xie et al. [27] for FO membranes. The pore

hindrance model that incorporates steric exclusion and hindered convection and diffusion was successfully used to estimate the membrane pore size, including nanofiltration and reverse osmosis membranes [28, 29], as well as FO membranes [27, 30, 31]. In this model, the membrane was considered as a bundle of cylindrical capillary tubes with the same radius. In addition, it was assumed that the spherical solute particles enter the membrane pores in random fashion. Specifically, the ratio of solute radius (r_s) to the membrane pore radius (r_p), $\lambda = r_s/r_p$, is related by the distribution coefficient φ when only steric interactions are considered:

$$\varphi = (1-\lambda)^2 \tag{4}$$

The real rejection of the organic tracers (R_r), which takes into account concentration polarisation, was determined from:

$$R_r = 1 - \frac{c_L}{c_o} = 1 - \frac{\varphi K_c}{1 - \exp(-P_e)(1-\varphi K_c)} \tag{5}$$

where c_o and c_L are the solute concentration just outside the pore entrance and pore exit, respectively; φ is the distribution coefficient for hard-sphere particles when only steric interactions are considered; K_c is the hydrodynamic hindrance coefficient for convection; and P_e is the membrane Peclet number defined as:

$$Pe = \frac{K_c J_v l}{K_d D \varepsilon} \tag{6}$$

Here, K_d is the hydrodynamic hindrance coefficient for diffusion, J_v is the membrane volumetric permeate flux, D is the Stokes-Einstein diffusion coefficient, l is the theoretical pore length (i.e., active layer thickness), and ε is the effective porosity of the membrane active later. Details on the calculations of P_e, K_c and K_d are given elsewhere [28, 32]. The φK_c and φK_d are two hindrance factors accounting for solute convection and diffusion, respectively. These factors significantly depend on the ratio of solute radius (r_s) to the membrane pore radius (r_p), λ.

The real rejection in Eq. 5 is linked to the observed rejection R_o using the film theory which accounts for concentration polarization:

$$\ln\frac{(1-R_r)}{R_r} = \ln\left(\frac{1-R_o}{R_o}\right) - \frac{J_v}{k_f} \tag{7}$$

where k_f is the mass transfer coefficient and J_v is the water permeate flux. A detailed, step-by-step flow chart for determination of FO and RO membrane average pore radii was showed in Figure S3, Supplementary Data.

2.3. Forward osmosis (FO) – reverse osmosis (RO) system

The FO-RO system used in this study consisted of an FO membrane cell, an RO membrane cell, circulation gear pumps for FO process, a positive displacement pump for RO filtration, and temperature control equipment (Supplementary Data, Figures S1).

The FO and RO membrane cells have identical dimensions. The FO membrane cell was made of acrylic plastic and designed to hold a flat-sheet membrane under moderate pressure differential without any physical support. The flow channels were engraved in the acrylic blocks that make up the feed and permeate semi-cells. Each channel was 2 mm deep, 90 mm wide, and 120 mm long. The RO membrane cell was a rectangular stainless-steel crossflow cell, with an effective membrane area of 110 cm^2 (10 cm × 11 cm) with a channel height of 2 mm.

In the FO-RO system, the draw solution reservoir of the FO process was also the feed reservoir for the RO process. Variable speed gear pumps (Micropump, Vancouver, WA) were used to circulate feed and draw solutions at a cross-flow velocity of 9 cm/s. A Hydra-Cell pump (Wanner Engineering Inc., Minneapolis, MN) was used to circulate the draw solution for RO filtration. The feed solution temperature was maintained at 25 °C using a water bath (Neslab RTE 7, Thermo Scientific, Waltham, MA). Weight changes of the draw and RO permeate reservoirs were recorded by digital balances (Mettler Toledo, Hightstown, NJ) connected to a computer.

2.4. Experimental protocol for FO-RO system operation

The sludge centrate feed was processed by the FO-RO system, achieving 14 litres of permeate water. The initial volumes of sludge centrate feed and draw solutions were 4 and 1 litres, respectively. The sludge centrate feed was replenished in batch mode to ensure relatively stable feed solution chemistry during the operation of the FO-RO system. Specifically, 2 L of sludge centrate feed was introduced to the feed tank when the 50% water recovery by the FO-RO system was achieved (i.e., two litres product water). For the FO process (active layer faced feed solution), 0.6 M NaCl draw solution generated a water flux of 20 L m^{-2} h^{-1}. In the RO process, the same water flux was obtained at a hydraulic pressure

of 58 bar. Water flux of the FO-RO system was recorded continuously. During the operation, the draw solution was not replenished in order to examine the passage and subsequent accumulation in the draw solution. The RO process continuously concentrated the diluted draw solution to the required concentration of 0.6 M NaCl (periodically monitored by the conductivity meter).

FO membrane flushing was conducted for each permeate volume of 2 L, where the FO membrane was flushed by deionised water at a doubled crossflow velocity (i.e., 18 cm/s) for 30 min. After FO membrane flushing, the sludge centrate feed was replenished to 4 litres. Feed, draw, and permeate samples were taken at specific time intervals for characterisation.

2.5. Feed, draw and permeate water characterisations

2.5.1. Water quality

Feed, draw and permeate water samples were subjected to a comprehensive water quality analysis, including pH, conductivity, total organic carbon (TOC), ultraviolet (UV) absorbance at 254 nm (UV_{254}) and 220 nm (UV_{220}), ammonium and phosphate. Specifically, TOC was measured using a total organic carbon analyser (TOC-$V_{CPH/CPN}$) (Shimadzu, Japan). UV_{220}, UV_{254} and concentrations of ammonium and phosphate were measured using a Hach DR 5000 spectrophotometer following standard methods.

2.5.2. Fluorescence excitation-emission matrix spectroscopy

Fluorescence intensities of feed, draw and permeate samples at 20 °C were measured for excitation wavelengths between 240 and 450 nm and emission wavelengths between 290 and 580 nm (in 5 nm increments) with a scanning fluorescence spectrophotometry (Perkin-Elmer LS-55). Samples were prepared and analysed according to Cory and McKnight [33], and Ohno [34]. Fluorophores detected at specific wavelength pairs within an excitation-emission-intensity matrix (EEM) are related to specific fractions of dissolved organic matter based on previous studies [35, 36]. All samples were diluted to a TOC concentration of 2 mg/L for resolving and comparing of EEM spectra.

2.5.3. Size exclusion chromatography

Size exclusion chromatography (SEC) was used to separate and identify the molecular weight and distribution of dissolved organic matter in the feed, draw and permeate samples. The SEC analysis is the separation technique based on the molecular (solute) size of the

components. Separation is achieved by the differential exclusion from the pores of the packing material, of the sample molecules as they pass through a bed of porous particles. SEC was obtained by a liquid chromatography equipped with a UV-visible photodiode array (PDA) detector (λ = 200-800 nm) [37]. The water sample was separated by a TSK gel column (G3000 SW, Tosoh Bioscience, Japan) at room temperature, with a phosphate buffer (10 mM KH_2PO_4, 10 mM Na_2HPO_4) as the mobile phase. The column was operated with a flow-rate of 0.5 mL/min and a 100 μL injection volume. The SEC column was calibrated by a series of polystyrene sulphonate (PSS) standards, with molecular weights of 3420, 4600, 6200, 15650 and 39000 g/mol. These PSS standards have molecular weights that were significantly higher than organic matters; and thus, acetone, a neutral solute, was included as a low molecular weight standard. A linear equation of the form $log(MW) = a\text{-}b(t)$ was obtained with a coefficient of determination R^2>0.999 (Figure S2, Supplementary Data), where MW is the molecular weight; t is the peak retention time. The obtained SEC chromatography was plotted as a contour map to identify the major dissolved organic matter peaks, and UV intensities of wavelengths 220 nm and 254 nm were selected to demonstrate the molecular weight and distribution of humic-like and protein-like substances, respectively, in the water samples.

3. Results and Discussion

3.1. Characteristics of digested sludge feed

Constituents in the feed sludge centrate were characterised by fluorescence EEM and SEC chromatography (Figure 1), coupled with water quality analyses (Table 1). Generally, the digested sludge centrate was comprised of high concentrations of nutrients (ammonium and phosphate) as well as abundant dissolved organic matter, which was challenging for the double membrane barriers in the FO-RO system.

A close examination of the dissolved organic matter in the feed was performed by fluorescent EEM and SEC chromatography. Feed sludge centrate exhibited two strong signatures in the fluorescence EEM as peak C ($\lambda_{ex/em}$=320-360/390-460 nm) and peak T_1 ($\lambda_{ex/em}$=275-290/330-370 nm), respectively (Figure 1A). Specifically, fluorophores in peak C are associated with visible humic-like substances occurring in natural organic matter derived from plant material [38]; while that in peak T_1 was attributed to tryptophan and protein-like materials related to microbial activities [34, 36, 39].

Similar observations were obtained in the SEC chromatography where two significant fingerprints were identified at the wavelengths of 220 nm and 254 nm (Figure 1B), which were characteristic of amino groups and aromatic content [40], suggesting that peaks corresponds to protein- and humic-like substances, respectively. A close examination of the SEC chromatography also showed the markedly different molecular weight distribution of protein- and humic-like substances in the feed matrix (Figure 1C). Specifically, the molecular weight distribution of protein-like substances was narrow, ranging from 220 to 240 g/mol; while that of humic-like substances was broad, varying from 300 to 10,000 g/mol.

[Figure 1]

[Table 1]

3.2. Key membrane properties

Key membrane mass transport parameters – pure water permeability (A), salt (NaCl) permeability (B), and observed salt (NaCl) rejection – were plotted in Figure 2. The TFC FO membrane exhibited higher water permeability, and higher salt permeability (i.e., lower salt rejection) in comparison with the RO membrane. This trend was consistent with the permeability-selectivity trade-off in polymeric membrane where the higher water permeation comes at the cost of lower salt rejection [41].

[Figure 2]

The real rejection (R_r) of each organic tracer was determined from the observed rejections (R_o) by accounting for concentration polarisation effects using Eq. 7 and the mass transfer coefficient calculated from Eq. 3. The real rejections obtained at different permeate fluxes were used to calculate the membrane average membrane pore radius based on the membrane pore hindrance transport model presented earlier (Eq. 5). The parameters φK_c and P_e/J_v are uniquely related to R_r. Thus, they could be determined by fitting the reference organic solute rejection data to the model (Eq. 5) using an optimization procedure (Solver, Microsoft Excel). As the parameters φK_c and P_e/J_v can be expressed as a sole function of the variable λ (which is the ratio of solute radius (r_s) to membrane pore radius (r_p)), λ can be obtained for each organic tracer and the membrane. The membrane average pore radius was then calculated for each reference solute rejection data.

For each membrane, the membrane pore radii obtained from three organic tracers only slightly deviated from one to another (within 5%). Results reported in Table 2 show that the average pore radius of the FO membrane (0.42 nm) is larger than that of the RO membrane (0.34 nm). The estimated membrane pore radii also agreed with the membrane mass transport parameters (Figure 2) where the FO membrane with a relatively larger membrane pore radius (0.42 nm) demonstrated higher water permeability and lower salt (NaCl) rejection than the RO membrane with a smaller pore radius (0.34 nm).

Molecular weight cut-off curves for the FO and RO membrane was plotted using parameters obtained in Table 2 (Figure 3). Briefly, the average membrane pore radii obtained for the FO and RO membranes were translated to an approximate Stokes radius (radius of equivalent sphere) as well as molecular weight using the Wilke and Chang and the Stokes-Einstein equations. The estimated molecular weight cut-offs (90% solute rejection) for the FO and RO membranes were 250 and 180 g/mol, respectively. This result also agreed well with the better salt rejection by the RO membrane in comparison with the FO membrane.

This discrepancy in membrane mass transport parameters and, more importantly, in membrane pore radii and molecular weight cut-off between FO and RO membranes played an important role in contaminant accumulation in draw solution in the FO-RO system. Because the active layer of both FO and RO membrane used here is polyamide, it was expected that solute-membrane interactions of these two membranes are similar, thereby minimizing variations in solute mass transport through the membranes and the solute rejection based on surface charge, adsorption or hydrogen bonding effects. Indeed, the zeta potential measurements showed that there was marginal difference between FO and RO membranes (Figure S4, Supplementary Data). As such, it was hypothesized that contaminants that permeate through the FO but not the RO membrane can accumulate in the draw solution, resulting in a solute build-up in the draw solution, thereby deteriorating the productivity and product quality of the FO-RO process.

[Table 2]

[Figure 3]

3.3. FO-RO system performance

3.3.1. Water production

Stable water production by the FO-RO system was achieved when digested sludge centrate was processed (Figure 4). This insignificant water flux decline of RO membrane demonstrated the effectiveness and robustness of FO process as a pre-treatment barrier for subsequent fouling sensitive RO process.

For low quality digested sludge feed (Table 1), evident by high TOC concentration (1,647 mg/L) and abundant dissolved organic matter (Figure 1), significant water flux decline was observed for the FO process. Water flux decline in FO could be attributed to both feed salinity build-up and membrane fouling. Reverse diffusion of NaCl draw solute elevated feed salinity, thereby reducing the overall driving force (i.e., effective osmotic pressure difference) in FO. On the other hand, FO membrane fouling was largely reversible following membrane flushing with deionized water, which resulted in nearly complete water flux recovery (Figure 4A). This result further confirmed the low fouling propensity of FO in processing low quality feed streams [2, 3, 42]. In addition, the insignificant water flux decline (less than 8%) in the RO filtration was also observed after processing 14 litres digested sludge centrate, suggesting FO being an effective barrier for the downstream RO filtration.

[Figure 4]

3.3.2. Rejection of organic matters and nutrients

The FO-RO system effectively rejected (>95%) organic matter (indicated by TOC and UV_{254} and UV_{220} measurements) and inorganic salts (indicated by ammonium and phosphate), thereby leading to high quality product water (Figure 5). This high rejection was attributed to the double membrane barriers against the various contaminants, which agreed with previous studies [19, 22].

A distinctive difference between ammonium (86%) and phosphate (92%) rejection by the FO membrane was observed (Figure 5C). The high rejections of ammonium and phosphate reported here are consistent with previous studies [7, 43]. Both electrostatic interaction and steric hindrance governed the rejections of ammonium and phosphate in FO. FO membrane was negatively charged at the experimental pH [44]. Thus, electrostatic repulsion between negatively charged FO membrane surface and phosphate ion led to high

phosphate rejection. On the other hand, both ammonium and phosphate ions are hydrated in aqueous solution, and hydration of these two ions significantly increases their hydrated molecular sizes. Indeed, hydrated radii for ammonium and phosphate are 0.33 and 0.49 nm [45], respectively, which are comparable to or larger than the estimated FO membrane pore radius (0.42 nm) (Table 2). Varying solute sizes of ammonium and phosphate also affect their diffusivities through the FO and RO membrane based on the solution-diffusion theory. Indeed, ammonium ion possessing four-times lower diffusion coefficient (9.4×10^{-11} m^2s^{-1}) than phosphate solute (2.28×10^{-10} m^2s^{-1}) led to a lower membrane rejection. As a result, steric hindrance also played an important role in rejections of ammonium and phosphate.

The difference in FO and RO membrane rejections of organic matter and nutrients resulted in the accumulation of these contaminants in the draw solution (section 3.4). Subsequently, the accumulation of contaminants in the draw solution may compromise the overall system productivity and efficiency. This potential detrimental effect could be reflected by the passage of dissolved organic matter substances that were abundant in the digested sludge feed through FO and RO membranes, and the accumulation of dissolved organic matter in the draw solution as the cumulative permeate volume increases.

[Figure 5]

3.4. Contaminant accumulation in the draw solution

3.4.1. Draw solution water quality

Marked build-up of nutrient ions and organic matter in the draw solution was observed, and the concentrations increased as the cumulative permeate volume increased (Figure 6). This detrimental accumulation phenomenon was driven by the lower rejection of FO membrane in comparison with RO membrane in the FO-RO system. Indeed, previous studies modelled the contaminant accumulation in the FO-RO system [20, 21], and suggested that the elevated contaminant concentration in the draw solution could deteriorate product water quality.

The passage of dissolved organic matter and subsequent accumulation in the draw solution were evident by the increase in the UV absorbance at wavelengths of 220 and 254 nm, respectively (Figure 6B). In particular, UV_{220} exhibited a significantly higher contaminant accumulation than UV_{254}. This difference could be attributed to the different rejections of the FO and RO membranes (Figures 2, 3 and Table 2), as well as the different

molecular weight and distribution of dissolved organic matter in the digested sludge centrate feed (Figure 2). Specifically, dissolved organic matter that contributed to UV_{254} absorbance possessed high molecular weight from 400 to 10,000 g/mol, which was well rejected by the FO membrane with molecular weight cut-off at 250 g/mol. On the other hand, the organic matter that induced UV_{220} intensity exhibited a narrow molecular weight distribution at approximate 220 g/mol, which was lower than the FO membrane molecular weight cut-off (250 g/mol), but close to the RO membrane with molecular weight cut-off at 180 g/mol (Figure 3). As a result, it is hypothesized that the accumulation of dissolved organic matter in the FO-RO system was mainly driven by the virtues of steric hindrance (size exclusion) of the FO and RO membranes. Fluorescence EEM spectroscopy and SEC chromatography were employed to continuously examine the dissolved organic matter in the draw and permeate solution to provide further insights to this hypothesis.

[Figure 6]

3.4.2. Fluorescence EEM spectra

Fluorescence EEM spectra of draw solution and permeate samples collected continuously from FO-RO process are illustrated in Figure 7. The draw solution EEMs demonstrated that a much lower intensity of fluorophore response peaks previously identified in feed EEMs could be still present, particularly the protein-like substances (Figure 1). This suggests that a broad class of fluorophores can be effectively removed by the FO membrane; however a fraction of the dissolved organic matter was still able to transport through the FO membrane. For instance, the draw solution EEM spectra demonstrated the fluorophore peak T_1 ($\lambda_{ex/em}$=275-290/330-370 nm), corresponding to weight protein-like fluorophores (e.g., tryptophan or other types of amino acids with phenyl groups), were poorly rejected by the FO membrane. This observation also agreed with the aforementioned UV absorbance results (Figure 6).

[Figure 7]

Accumulation of fluorophores in the draw solution was further revealed by EEM spectra. The intensities of peaks *C* and T_1 (representative of fulvic- and protein-like substances, respectively) increased as the cumulative permeate volume increased (upper row, Figure 7). More importantly, the intensity of peak T_1 (protein-like substances) increased at a faster rate than that of peak *C* (visible humic-like substances). Such accumulation resulted in

409 discernible fluorescence signatures for peak T_1 as the amount of permeate processed
410 increased, which suggested the protein-like substances had low molecular weight.

411 *3.4.3. SEC chromatography*

412 The SEC chromatography further examined the dissolved organic matter that was
413 identified in the fluorescence EEM spectra (Figure 8), and shed light on the mechanism that
414 governs the passage and accumulation of dissolved organic matter in the FO-RO system. The
415 contour map of draw solution and permeate samples resolved the concentrations and
416 molecular weights of the dissolved organic matter that diffused through the FO and RO
417 membranes and accumulated in the draw solution (Figure 8).

418 **[Figure 8]**

419 SEC chromatography of draw solution illustrated a progressive increase in the peak
420 area at retention time of 48 minutes (upper row, Figure 8), corresponding to the solute
421 molecular weight of 200 g/mol, which was smaller than the estimated molecular weight cut-
422 off of FO membrane (250 g/mol). This result agreed with the steric hindrance (size exclusion)
423 mechanism, which played an important role in the passage and accumulation of dissolved
424 organic matters. This observation, together with fluorescence EEM spectra, suggested low
425 molecular weight, protein-like dissolved organic matters diffused through the FO membrane.
426 In addition, these low molecular weight protein-like substances also passed through the RO
427 membrane with molecular weight cut-off of 180 g/mol, enabling detection of small peaks at
428 50 minutes towards the conclusion of the FO-RO system operation (lower row, Figure 8).

429 SEC chromatography of draw solution and permeate obtained at wavelengths of 220
430 nm and 254 nm at the end of the FO-RO system operation provided further detail of the
431 composition of dissolved organic matter in the draw solution and product water (Figure 9).
432 Specifically, the dominant species in the draw solution exhibited strong absorbance at
433 wavelength of 220 nm, confirming the presence of protein-like substance, with molecular
434 weight of 200 g/mol (Figure 9A). It could be attributed to the steric hindrance (size
435 exclusion) mechanism in the FO mass transfer. It is also noteworthy that the small shoulder
436 peak showed at the retention time of 43 minutes, suggesting the presence of compounds with
437 molecular weight of 300 g/mol. This protein-like substance with larger molecular weight
438 might be due to the aggregation of protein-like substances in the draw solution. A much
439 smaller portion of humic-like substance also could be found in the draw solution at

wavelength of 254 nm, suggesting the molecular weight of 180 g/mol. Due to the accumulation of protein-like substances in the draw solution, the same peak with two orders of magnitude lower intensity was also identified in the product water (Figure 9B), which is of concern to the product water quality.

[Figure 9]

3.5 Implications

Transport and subsequent accumulation of contaminants in the FO-RO system reported here have significant implications for the management and advancement of the FO-based system. The accumulation of undesirable contaminants in the draw solution not only demands additional management of the draw solution, but also jeopardises the entire system productivity and performance. The robust, double-barrier concept of the FO-RO system can be compromised due to this detrimental contaminant accumulation. Indeed, several prior investigations either modelled this phenomenon or provided experimental evidence. For instance, D'Haese et al. [21] modelled the TrOC accumulation in an FO-RO hybrid system and predicted that an elevated TrOC concentration in the draw solution deteriorated the product water quality. Xie et al. [11, 12] reported the concentrations of organic matter and TrOCs in the draw solution increased substantially as the water recovery increased and proposed two strategies – activated carbon adsorption and ultra-violet oxidation – to mitigate this effect.

The transport and accumulation mechanisms elucidated here shed light on the mechanisms for contaminant build up in FO draw solutions and identifies the need for draw solution management when processing challenging waste streams [46]. In addition, the mechanisms highlighted here also open opportunity for development of high performance FO membrane, thereby reducing the margin in solute rejection between FO and RO membranes.

4. Conclusion

Results reported here demonstrated contaminant accumulation in the FO-RO system when processing digested sludge centrate that was abundant with nutrients and dissolved organic matter. Despite the high rejection of the FO-RO system, contaminant accumulation was evident by a progressive increase in the nutrient and dissolved organic matter in the draw solution. More importantly, the passage and accumulation of dissolved organic matter were identified and quantified by fluorescence EEM spectra and SEC chromatography to elucidate

the mechanism for the detrimental accumulation phenomenon. The major constituent that accumulated in the draw solution exhibited a distinct signature in the fluorescence EEM spectra at peak T_1 ($\lambda_{ex/em}$=275-290/330-370 nm), suggesting protein-like substance. The molecular weight of the protein-like substance was examined by SEC chromatography, indicating a molecular weight of 200 g/mol. This observation agreed well with the estimated FO (0.42 nm, with molecular weight cut-off at 250 g/mol) and RO (0.34nm, with molecular weight cut-off at 180 g/mol) membrane pore radii. The low molecular weight protein-like substance diffused through the FO membrane, and was mainly rejected by the RO membrane by the virtue of steric hindrance (i.e., size exclusion) mechanism. This contaminant accumulation phenomenon may affect the productivity and sustainability of the FO-RO system.

5. Acknowledgment

The Victoria University is thanked for the award of a Vice Chancellor Early Career Fellowship to M.X..

6. References

[1] R. Valladares Linares, Z. Li, S. Sarp, S.S. Bucs, G. Amy, J.S. Vrouwenvelder, Forward osmosis niches in seawater desalination and wastewater reuse, Water Research, 66 (2014) 122-139.

[2] B. Mi, M. Elimelech, Chemical and physical aspects of organic fouling of forward osmosis membranes, Journal of Membrane Science, 320 (2008) 292-302.

[3] B. Mi, M. Elimelech, Organic fouling of forward osmosis membranes: Fouling reversibility and cleaning without chemical reagents, Journal of Membrane Science, 348 (2010) 337-345.

[4] C. Boo, M. Elimelech, S. Hong, Fouling control in a forward osmosis process integrating seawater desalination and wastewater reclamation, Journal of Membrane Science, 444 (2013) 148-156.

[5] S. Lee, C. Boo, M. Elimelech, S. Hong, Comparison of fouling behavior in forward osmosis (FO) and reverse osmosis (RO), Journal of Membrane Science, 365 (2010) 34-39.

[6] J.R.B. Herron, Edward G. Salter, Robert, Direct osmotic concentration contaminated water, in, OSMOTEK, INC., 1997.

[7] R.W. Holloway, A.E. Childress, K.E. Dennett, T.Y. Cath, Forward osmosis for concentration of anaerobic digester centrate, Water Research, 41 (2007) 4005-4014.

[8] A. Achilli, T.Y. Cath, E.A. Marchand, A.E. Childress, The forward osmosis membrane bioreactor: A low fouling alternative to MBR processes, Desalination, 239 (2009) 10-21.

[9] E.R. Cornelissen, D. Harmsen, K.F. de Korte, C.J. Ruiken, J.-J. Qin, H. Oo, L.P. Wessels, Membrane fouling and process performance of forward osmosis membranes on activated sludge, Journal of Membrane Science, 319 (2008) 158-168.

[10] T.Y. Cath, S. Gormly, E.G. Beaudry, M.T. Flynn, V.D. Adams, A.E. Childress, Membrane contactor processes for wastewater reclamation in space: Part I. Direct osmotic concentration as pretreatment for reverse osmosis, Journal of Membrane Science, 257 (2005) 85-98.

[11] M. Xie, L.D. Nghiem, W.E. Price, M. Elimelech, Toward Resource Recovery from Wastewater: Extraction of Phosphorus from Digested Sludge Using a Hybrid Forward Osmosis–Membrane Distillation Process, Environmental Science & Technology Letters, 1 (2014) 191-195.

[12] M. Xie, L.D. Nghiem, W.E. Price, M. Elimelech, A Forward Osmosis–Membrane Distillation Hybrid Process for Direct Sewer Mining: System Performance and Limitations, Environmental Science & Technology, 47 (2013) 13486-13493.

[13] C.H. Tan, H.Y. Ng, A novel hybrid forward osmosis - nanofiltration (FO-NF) process for seawater desalination: Draw solution selection and system configuration, Desalination and Water Treatment, 13 (2010) 356-361.

[14] O.A. Bamaga, A. Yokochi, B. Zabara, A.S. Babaqi, Hybrid FO/RO desalination system: Preliminary assessment of osmotic energy recovery and designs of new FO membrane module configurations, Desalination, 268 (2011) 163-169.

[15] V. Yangali-Quintanilla, Z. Li, R. Valladares, Q. Li, G. Amy, Indirect desalination of Red Sea water with forward osmosis and low pressure reverse osmosis for water reuse, Desalination, 280 (2011) 160-166.

[16] N.T. Hancock, P. Xu, D.M. Heil, C. Bellona, T.Y. Cath, Comprehensive Bench- and Pilot-Scale Investigation of Trace Organic Compounds Rejection by Forward Osmosis, Environmental Science & Technology, 45 (2011) 8483-8490.

[17] Q. Ge, P. Wang, C. Wan, T.-S. Chung, Polyelectrolyte-Promoted Forward Osmosis–Membrane Distillation (FO–MD) Hybrid Process for Dye Wastewater Treatment, Environmental Science & Technology, 46 (2012) 6236-6243.

[18] K.Y. Wang, M.M. Teoh, A. Nugroho, T.-S. Chung, Integrated forward osmosis–membrane distillation (FO–MD) hybrid system for the concentration of protein solutions, Chemical Engineering Science, 66 (2011) 2421-2430.

[19] N.T. Hancock, P. Xu, M.J. Roby, J.D. Gomez, T.Y. Cath, Towards direct potable reuse with forward osmosis: Technical assessment of long-term process performance at the pilot scale, Journal of Membrane Science, 445 (2013) 34-46.

[20] D.L. Shaffer, N.Y. Yip, J. Gilron, M. Elimelech, Seawater desalination for agriculture by integrated forward and reverse osmosis: Improved product water quality for potentially less energy, Journal of Membrane Science, 415–416 (2012) 1-8.

[21] A. D'Haese, P. Le-Clech, S. Van Nevel, K. Verbeken, E.R. Cornelissen, S.J. Khan, A.R.D. Verliefde, Trace organic solutes in closed-loop forward osmosis applications: Influence of membrane fouling and modeling of solute build-up, Water Research, 47 (2013) 5232-5244.

[22] Z.-Y. Li, V. Yangali-Quintanilla, R. Valladares-Linares, Q. Li, T. Zhan, G. Amy, Flux patterns and membrane fouling propensity during desalination of seawater by forward osmosis, Water Research, 46 (2012) 195-204.

[23] R. Valladares Linares, V. Yangali-Quintanilla, Z. Li, G. Amy, NOM and TEP fouling of a forward osmosis (FO) membrane: Foulant identification and cleaning, Journal of Membrane Science, 421–422 (2012) 217-224.

[24] R.L. McGinnis, N.T. Hancock, M.S. Nowosielski-Slepowron, G.D. McGurgan, Pilot demonstration of the NH3/CO2 forward osmosis desalination process on high salinity brines, Desalination, 312 (2013) 67-74.

[25] T.Y. Cath, M. Elimelech, J.R. McCutcheon, R.L. McGinnis, A. Achilli, D. Anastasio, A.R. Brady, A.E. Childress, I.V. Farr, N.T. Hancock, J. Lampi, L.D. Nghiem, M. Xie, N.Y. Yip, Standard Methodology for Evaluating Membrane Performance in Osmotically Driven Membrane Processes, Desalination, 312 (2013) 31-38.

[26] I. Sutzkover, D. Hasson, R. Semiat, Simple technique for measuring the concentration polarization level in a reverse osmosis system, Desalination, 131 (2000) 117-127.

[27] M. Xie, L.D. Nghiem, W.E. Price, M. Elimelech, Comparison of the removal of hydrophobic trace organic contaminants by forward osmosis and reverse osmosis, Water Research, 46 (2012) 2683-2692.

[28] L.D. Nghiem, A.I. Schäfer, M. Elimelech, Removal of Natural Hormones by Nanofiltration Membranes: Measurement, Modeling, and Mechanisms, Environmental Science & Technology, 38 (2004) 1888-1896.

[29] M.J. López-Muñoz, A. Sotto, J.M. Arsuaga, B. Van der Bruggen, Influence of membrane, solute and solution properties on the retention of phenolic compounds in aqueous solution by nanofiltration membranes, Separation and Purification Technology, 66 (2009) 194-201.

[30] M. Xie, L.D. Nghiem, W.E. Price, M. Elimelech, Relating rejection of trace organic contaminants to membrane properties in forward osmosis: Measurements, modelling and implications, Water Research, 49 (2014) 265-274.

[31] W. Luo, M. Xie, F.I. Hai, W.E. Price, L.D. Nghiem, Biodegradation of cellulose triacetate and polyamide forward osmosis membranes in an activated sludge bioreactor: Observations and implications, Journal of Membrane Science, 510 (2016) 284-292.

[32] P.M. Bungay, H. Brenner, The motion of a closely-fitting sphere in a fluid-filled tube, International Journal of Multiphase Flow, 1 (1973) 25-56.

[33] R.M. Cory, D.M. McKnight, Fluorescence Spectroscopy Reveals Ubiquitous Presence of Oxidized and Reduced Quinones in Dissolved Organic Matter, Environmental Science & Technology, 39 (2005) 8142-8149.

[34] T. Ohno, Fluorescence Inner-Filtering Correction for Determining the Humification Index of Dissolved Organic Matter, Environmental Science & Technology, 36 (2002) 742-746.

[35] R.K. Henderson, A. Baker, K.R. Murphy, A. Hambly, R.M. Stuetz, S.J. Khan, Fluorescence as a potential monitoring tool for recycled water systems: A review, Water Research, 43 (2009) 863-881.

589 [36] N. Her, G. Amy, D. McKnight, J. Sohn, Y. Yoon, Characterization of DOM as a
590 function of MW by fluorescence EEM and HPLC-SEC using UVA, DOC, and fluorescence
591 detection, Water Research, 37 (2003) 4295-4303.

592 [37] B.P. Allpike, A. Heitz, C.A. Joll, R.I. Kagi, G. Abbt-Braun, F.H. Frimmel, T.
593 Brinkmann, N. Her, G. Amy, Size Exclusion Chromatography To Characterize DOC
594 Removal in Drinking Water Treatment, Environmental Science & Technology, 39 (2005)
595 2334-2342.

596 [38] P.G. Coble, Characterization of marine and terrestrial DOM in seawater using
597 excitation-emission matrix spectroscopy, Marine Chemistry, 51 (1996) 325-346.

598 [39] N. Hudson, A. Baker, D. Reynolds, Fluorescence analysis of dissolved organic matter in
599 natural, waste and polluted waters—a review, River Research and Applications, 23 (2007)
600 631-649.

601 [40] N. Her, G. Amy, H.-R. Park, M. Song, Characterizing algogenic organic matter (AOM)
602 and evaluating associated NF membrane fouling, Water Research, 38 (2004) 1427-1438.

603 [41] G.M. Geise, H.B. Park, A.C. Sagle, B.D. Freeman, J.E. McGrath, Water permeability
604 and water/salt selectivity tradeoff in polymers for desalination, Journal of Membrane Science,
605 369 (2011) 130-138.

606 [42] M. Xie, L.D. Nghiem, W.E. Price, M. Elimelech, Impact of humic acid fouling on
607 membrane performance and transport of pharmaceutically active compounds in forward
608 osmosis, Water Research, 47 (2013) 4567-4575.

609 [43] N.C. Nguyen, S.-S. Chen, H.-Y. Yang, N.T. Hau, Application of forward osmosis on
610 dewatering of high nutrient sludge, Bioresource Technology, 132 (2013) 224-229.

611 [44] M. Xie, W.E. Price, L.D. Nghiem, Rejection of pharmaceutically active compounds by
612 forward osmosis: Role of solution pH and membrane orientation, Separation and Purification
613 Technology, 93 (2012) 107-114.

614 [45] E.R. Nightingale, Phenomenological Theory of Ion Solvation. Effective Radii of
615 Hydrated Ions, The Journal of Physical Chemistry, 63 (1959) 1381-1387.

616 [46] M. Xie, H.K. Shon, S.R. Gray, M. Elimelech, Membrane-based processes for wastewater
617 nutrient recovery: Technology, challenges, and future direction, Water research, 89 (2016)
618 210-221.

619

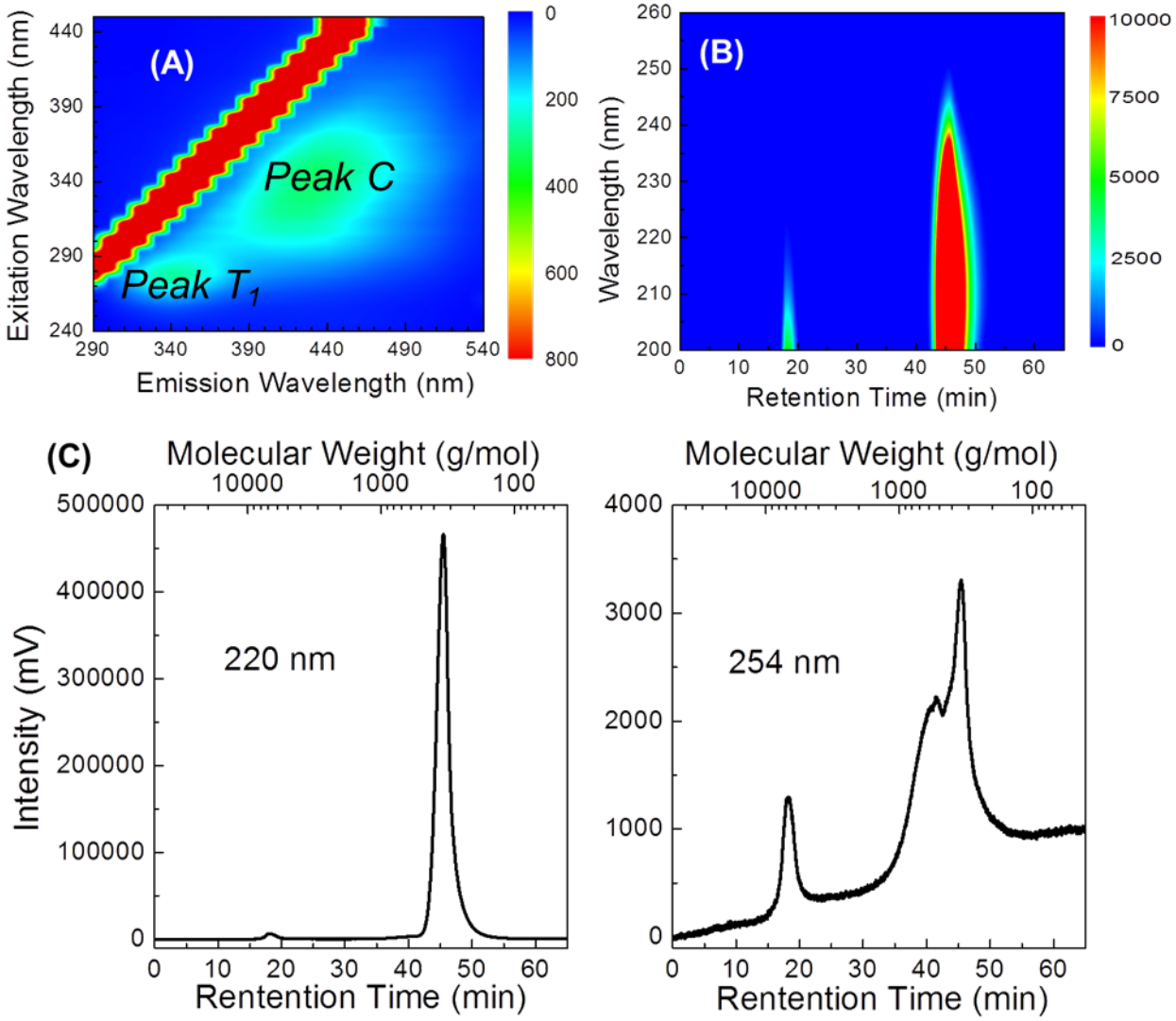

620

621

622 **Figure 1:** Characteristics of digested sludge feed by (A) fluorescence excitation-emission
623 matrix spectroscopy with peak *C* and peak T_1; (B) size exclusion chromatography with UV-
624 visible photodiode array (PDA) detector in a contour map, and (C) size exclusion
625 chromatography at wavelengths of 220 nm and 254 nm as a function of molecular weight
626 distribution.

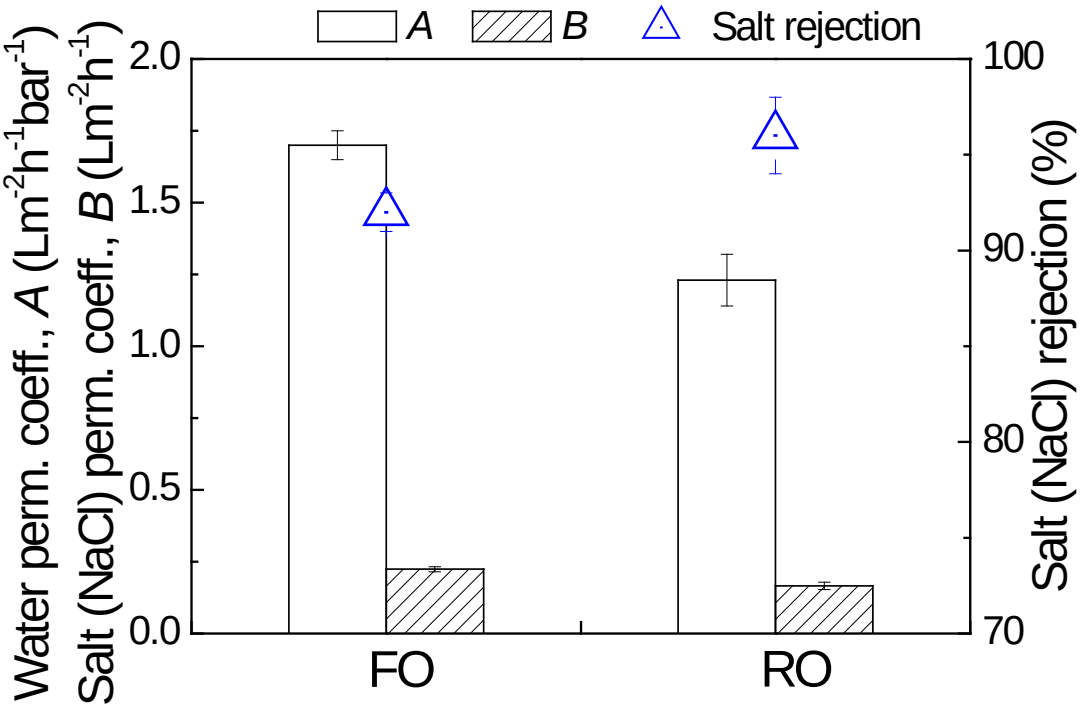

627

628

629 **Figure 2:** Key mass transfer parameters, water and salt (NaCl) permeability coefficients, and
630 observed NaCl rejection for the FO and RO membranes Error bars represent standard
631 deviation from duplication measurements of two membrane samples.

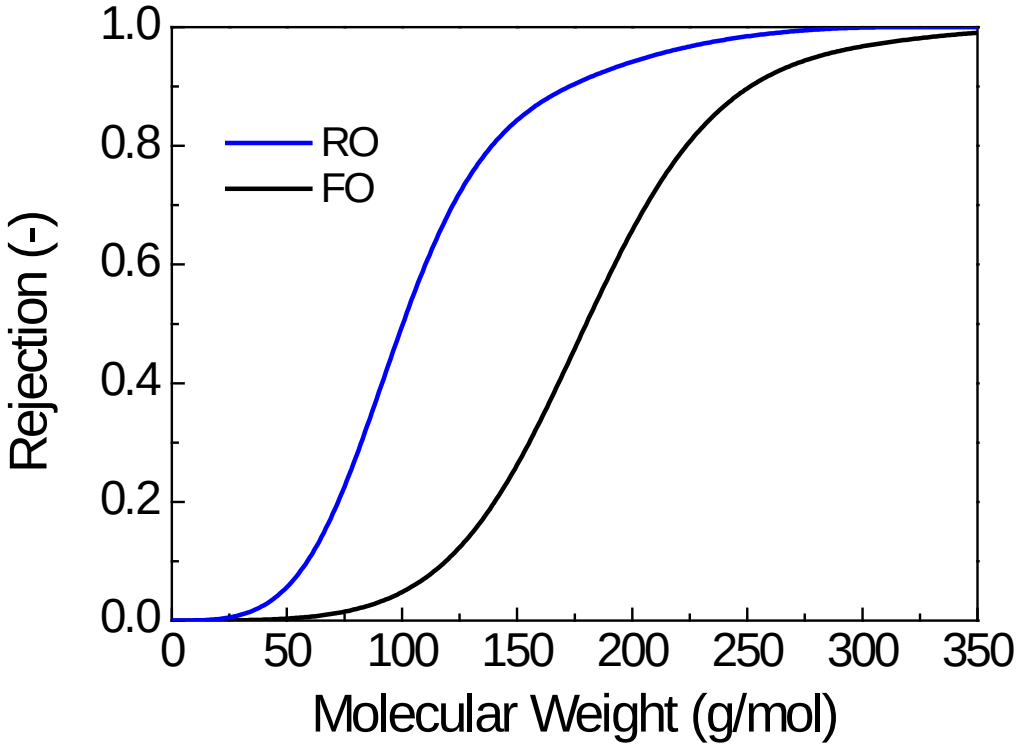

Figure 3: The modelled rejections of FO and RO membranes as a function of molecular weight based on the pore hindrance model (Equation 5). The relevant organic tracer parameters in Table 2 were used in the model calculations. The molecular weight was translated to an approximate Stokes radius (radius of equivalent sphere) using the Wilke and Chang and the Stokes-Einstein equations.

Table 1: Key physicochemical properties of digested sludge centrate (average ± standard deviation from duplicate measurements)

Parameter	Value
Turbidity (NTU)	59 ± 9
Electrical Conductivity (mS/cm)	2.72 ± 0.12
pH (-)	7.12 ± 0.02
Total organic carbon (mg/L)	1,847 ± 20
Ammonium (mg/L)	838 ± 25
Phosphate (mg/L)	323 ± 12
UV_{254} (cm^{-1}) [1]	0.85 ± 0.02
UV_{220} (cm^{-1}) [1]	0.69 ± 0.01

[1] feed sample was diluted by 50 times with deionised water, and was measured using a 1 cm quartz cuvette.

641 **Table 2**: Estimated average membrane pore radii for FO and RO membranes obtained from
642 organic tracer experiments

Organic tracer	Solute size [1] r_s (nm)	$\lambda=r_s/r_p$	Pore radius r_p (nm)	Pore length/porosity, l/ε (µm)
RO membrane				
Erythitol	0.26	0.79	0.33	3.08
Xylose	0.29	0.86	0.34	1.74
Glucose	0.32	0.89	0.36	1.03
Average			0.34	1.95
FO membrane				
Erythitol	0.26	0.63	0.41	0.08
Xylose	0.29	0.69	0.42	0.18
Glucose	0.32	0.75	0.43	0.11
Average			0.42	0.12

643 [1] calculated from estimated membrane pore radius using Stokes equation

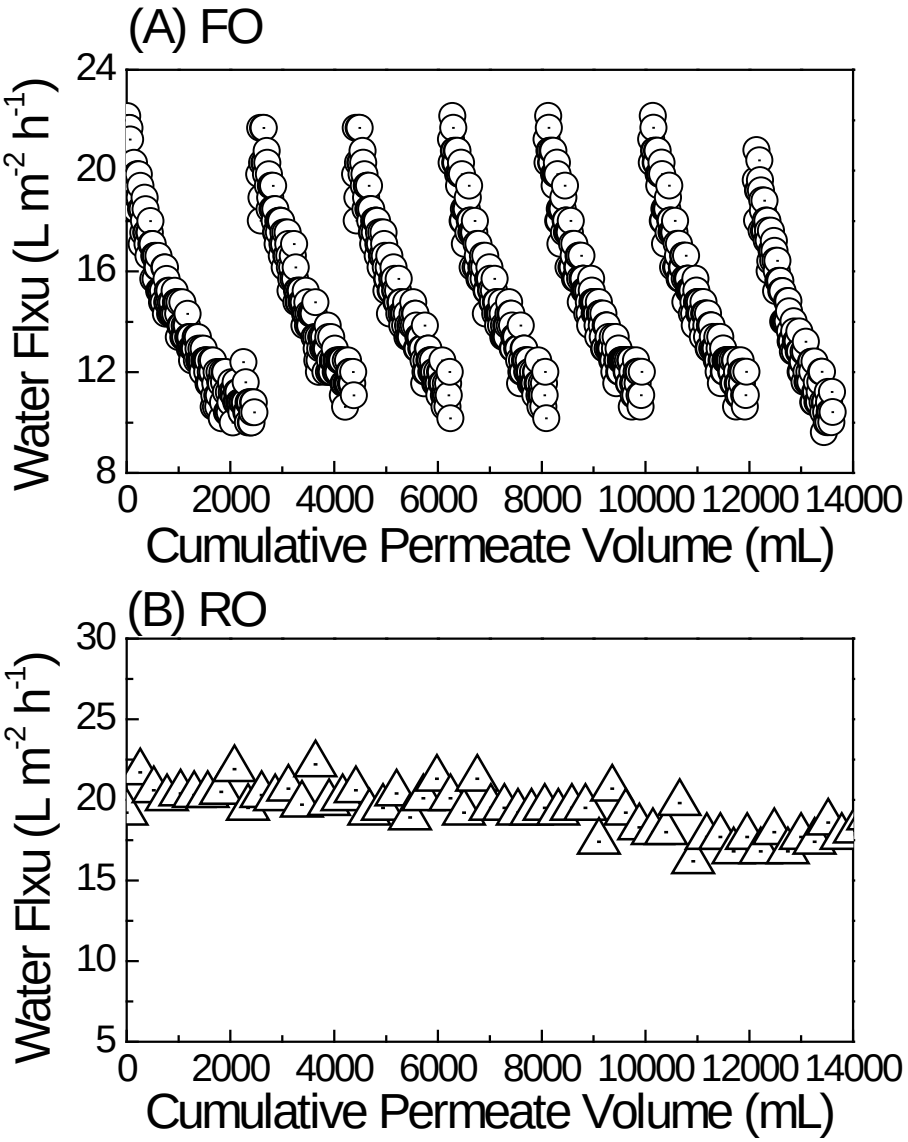

644

645

646 **Figure 4:** Water production by the FO – RO system: (A) FO and (B) RO process.
647 Experimental conditions: digested sludge centrate feed (Table 1); draw solution of 0.6 M
648 NaCl; temperatures of feed and draw were 20 °C; and cross-flow rates of 1 L/min
649 (corresponding to cross-flow velocity of 9 cm/s) for the feed and draw. FO membrane
650 flushing was conducted when water flux decreased to 50% of its initial value. Deionized
651 water was used to flush the fouled FO membrane for 30 min at a cross-flow velocity of 18
652 cm/s. RO process was operated at the hydraulic pressure of 28 bar (406 psi) using SW30 RO
653 membrane at RO feed (i.e., draw from FO process) temperature of 20 °C, the cross-flow rate
654 of the RO feed was 1 L/min (corresponding to cross-flow velocity of 9 cm/s).

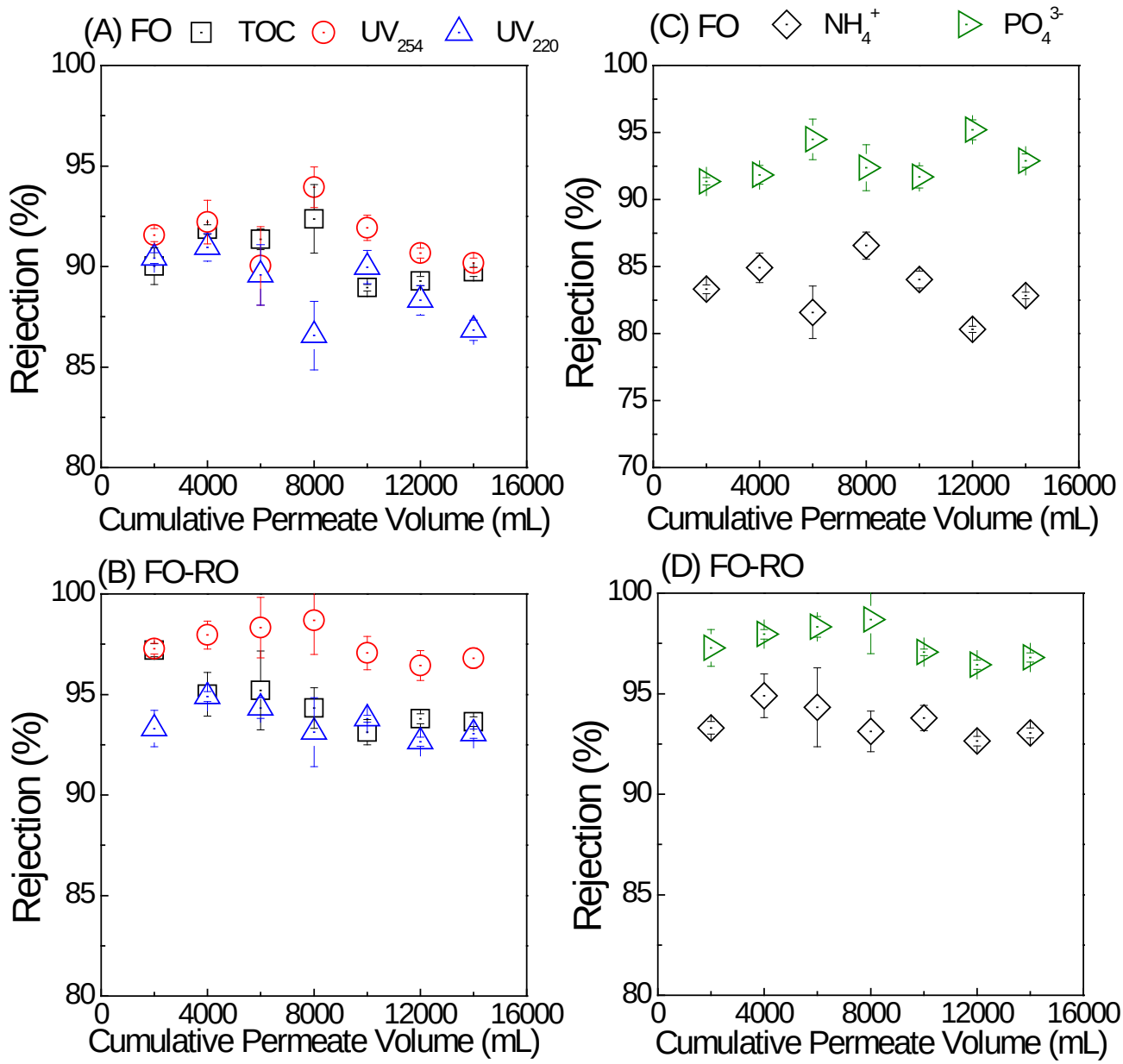

Figure 5: Rejections of total organic carbon (TOC), and UV_{220}, UV_{254} absorbance by (A) FO process, and (B) FO-RO process; and rejections of ammonium and phosphate by (C) FO process, and (D) FO-RO process, as a function of cumulative permeate volume. Experimental conditions are described in Figure 1.

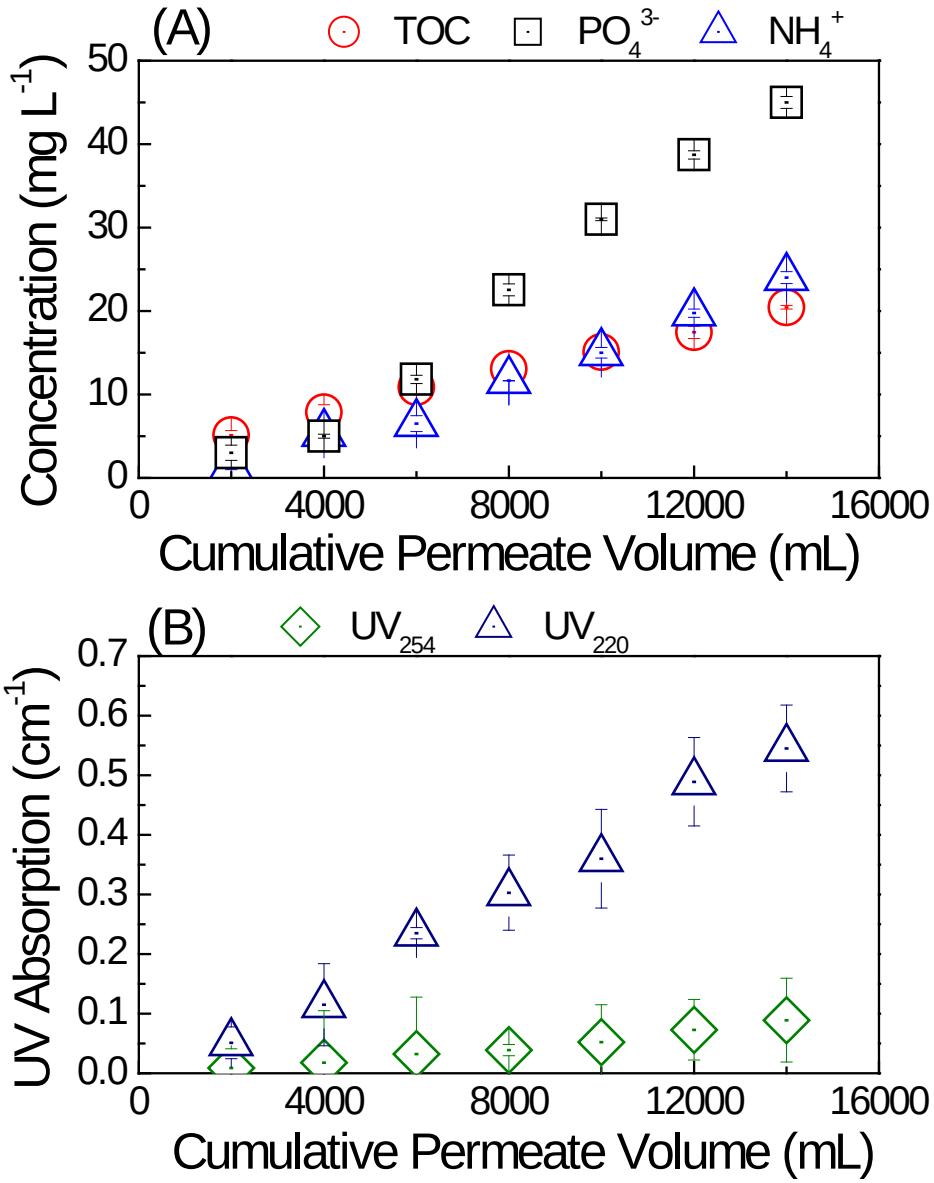

661

662

663 **Figure 6: (A)** Concentrations of total organic carbon (TOC), ammonium, and phosphate in
664 the draw solution as a function of cumulative permeate volume; and (B) UV absorbance at
665 wavelengths of 220 nm (UV_{220}) and 254 nm (UV_{254}) in the draw solution as a function of
666 cumulative permeate volume. Error bars represent standard deviation from duplicate
667 measurements. Experimental conditions were described in Figure 1.

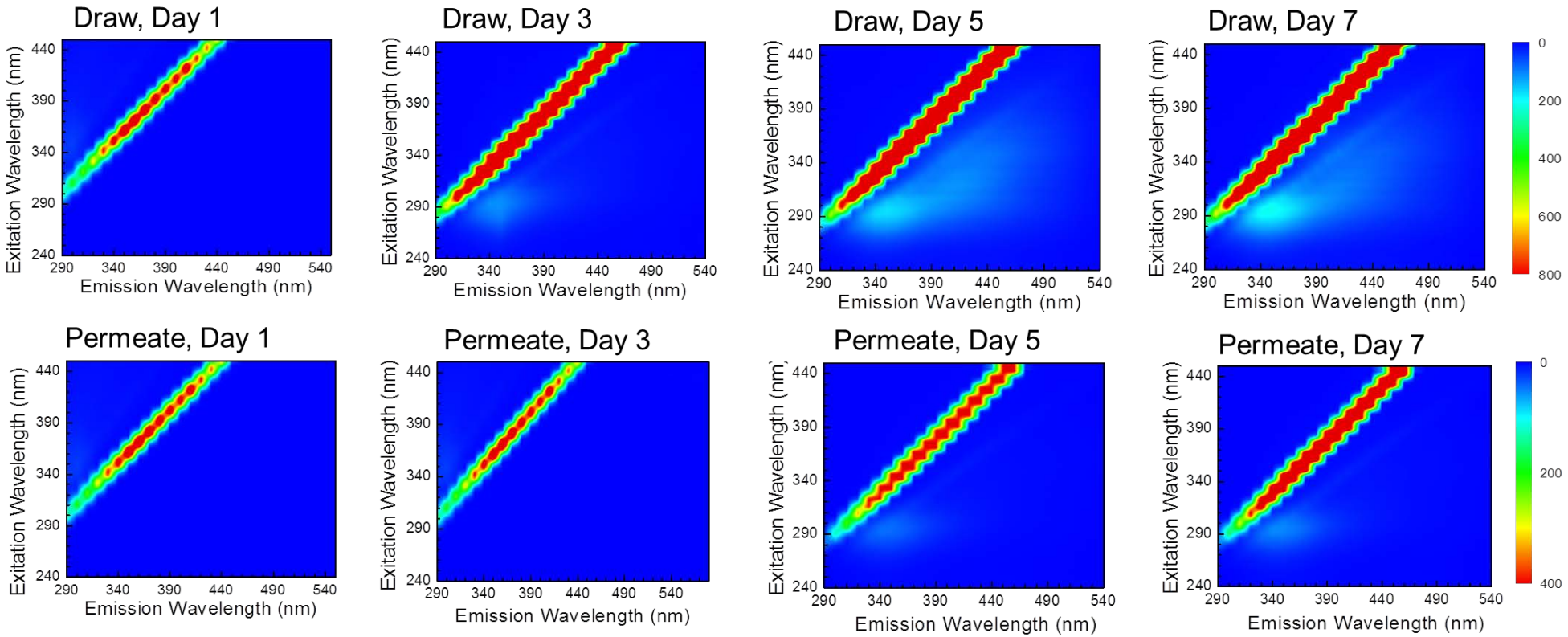

668

669

670 **Figure 7:** Fluorescence excitation and emission matrix (EEM) spectra for draw (upper row) and permeate (lower row) solutions at specific time
671 intervals (day 1, 3, 5 and 7). Total organic carbon concentrations for all solutions were normalised to 5 mg/L for comparison. EEM spectra were
672 collected at excitation wavelengths between 240 and 450 nm, and emission wavelengths between 290 and 580 nm (in 5 nm increment). The
673 fluorescent intensity scaling bar for draw solution (0 to 800) was twice larger than that for permeate (0 to 400).

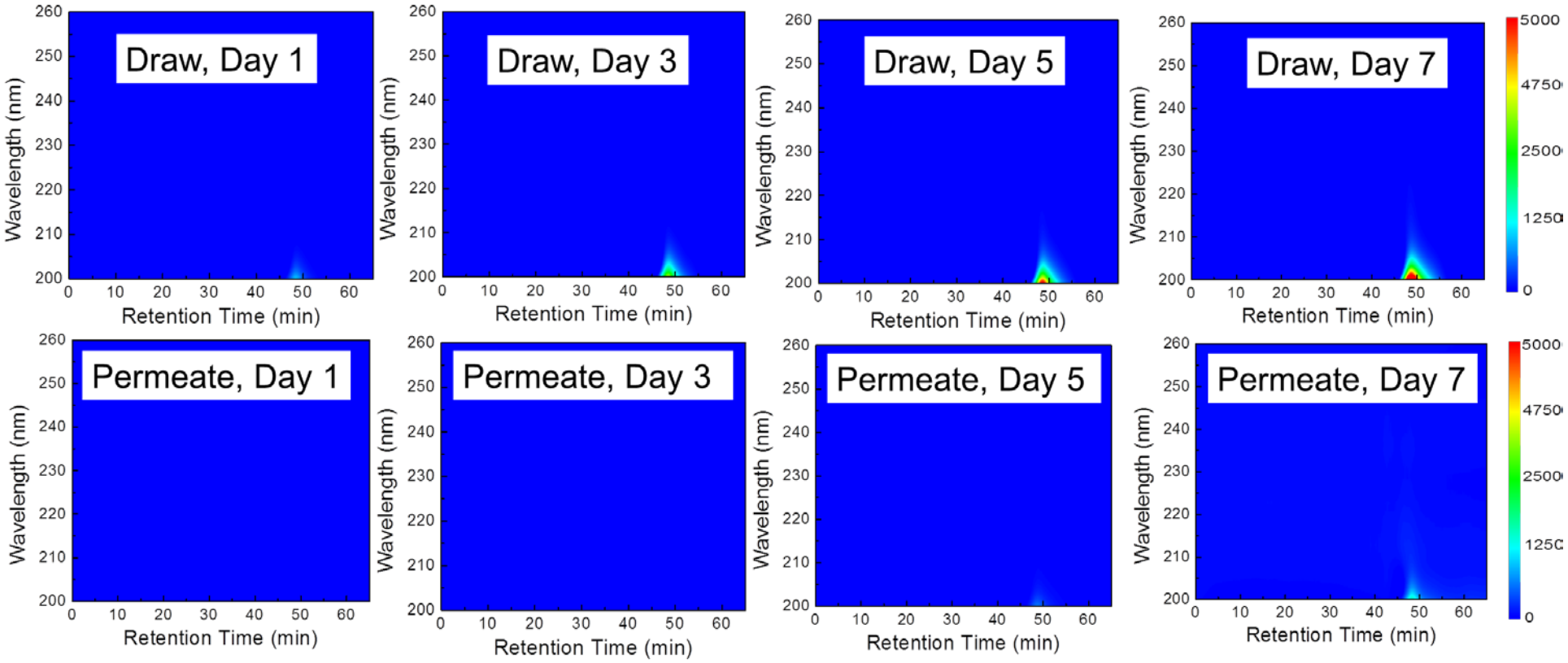

Figure 8: Size exclusion (SEC) chromatography for draw (upper row) and permeate (lower row) solutions at specific time intervals (day 1, 3, 5 and 7). The SEC chromatographs were plotted as a contour map. SEC chromatography was obtained by a liquid chromatography equipped with a UV-visible photodiode array (PDA) detector (λ = 200-800 nm), using a size exclusion gel column (G3000 SW, Tosoh Bioscience, Japan) at room temperature, with a phosphate buffer (10 mM KH_2PO_4, 10 mM Na_2HPO_4) as the mobile phase.

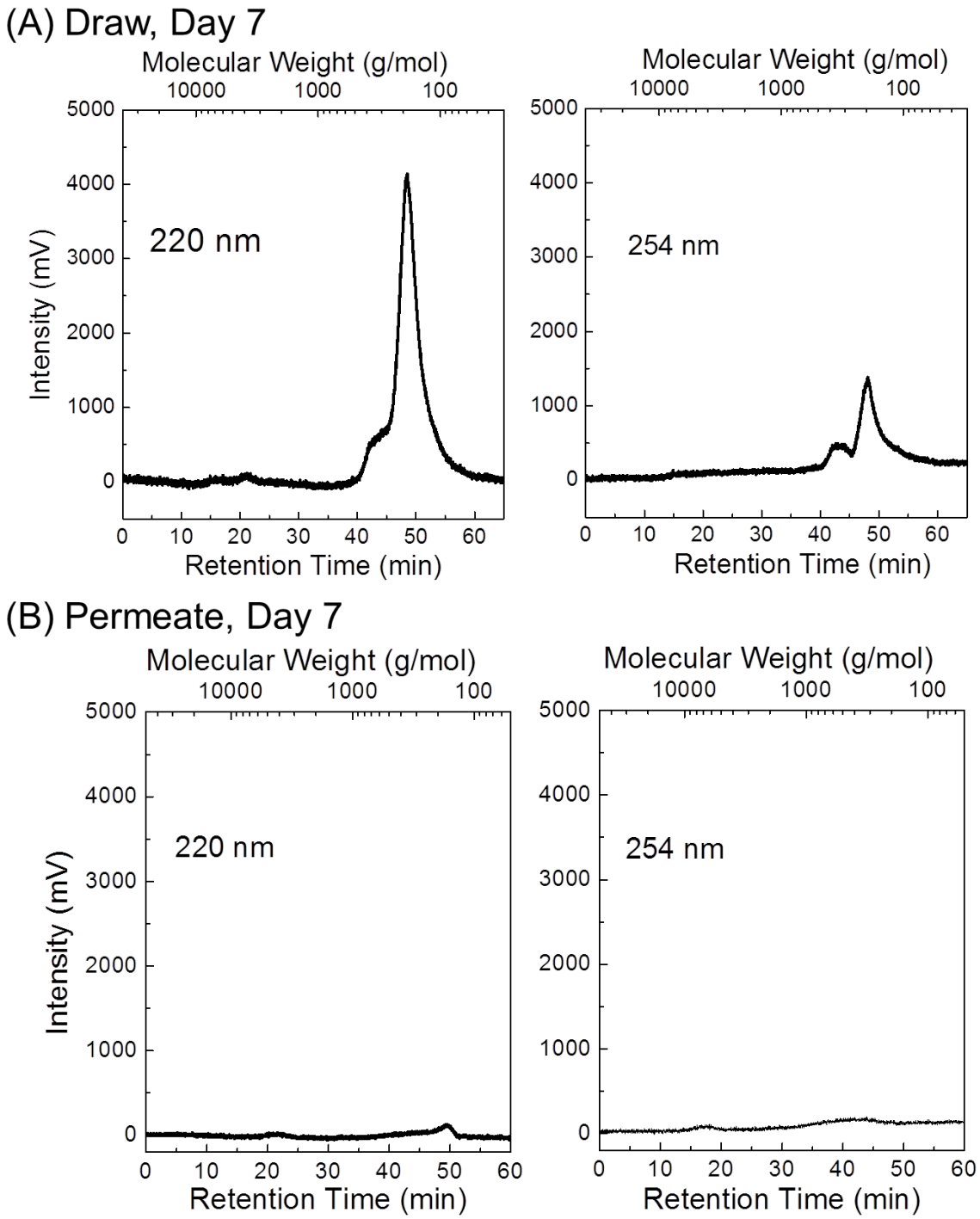

680

681

682 **Figure 9:** Size exclusion chromatography for (A) draw solution, and (B) permeate, at
683 wavelengths of 220 nm and 254 nm at the conclusion of the FO-RO operation. The molecular
684 weight was calibrated as peak retention time using polystyrene sulphonate with a series of
685 molecular weight. SEC chromatography conditions were described in Figure 8.